CHINESE OPTICS LETTERS

Vol. 22, No. 5 | May 2024

Smart beam via electrically addressing the dye-doped and polymer-stabilized cholesteric liquid crystals

Cheng Peng (彭 程), Chunting Xu (徐春庭)*, and Wei Hu (胡 伟)**

College of Engineering and Applied Sciences, Nanjing University, Nanjing 210023, China

*Corresponding author: xuchunting@nju.edu.cn

**Corresponding author: huwei@nju.edu.cn

Received November 20, 2023 | Accepted January 22, 2024 | Posted Online May 17, 2024

Smart beams play a vital role in modern intelligent vehicles and have recently attracted significant attention. A spatial light modulator with high optical efficiency, low cost, and compact size is crucial for designing smart beams. Here, we mix cholesteric liquid crystals with dichroic black dye and a monomer. After UV polymerization, the sample exhibits a low driving voltage of 26 V, a high transmittance of over 70%, and an On-off ratio over 280, thanks to the joint contribution of both the absorption and the scattering effect. A smart beam device is demonstrated by electrically addressing the dye-doped and polymer-stabilized cholesteric liquid crystal with pixelated electrodes. Light patterns with arbitrary designs are projected dynamically. The switching time reaches several tens of milliseconds. This strategy brings new designs to intelligent vehicles and may also inspire applications in public information displays, advertising, and even AR/VR displays.

Keywords: cholesteric liquid crystal; spatial light modulation; smart beam; dye; guest-host effect.

DOI: 10.3788/COL202422.053301

1. Introduction

Recently, with the rapid development of artificial intelligence, intelligent vehicles have attracted significant attention from both academic and industrial fields[1–3]. An increasing number of high-tech technologies, such as sensing, LiDAR, and automatic control, have been adopted in this region[4,5]. High-energy directional beams penetrate the cornea and crystalline lens of human eyes and may cause photochemical reactions inside the retina, leading to temporal or even permanent visual impairments[6]. In particular, the far beams of vehicles during nighttime driving may cause temporary blindness to oncoming traffic and pedestrians, greatly increasing the risk of traffic accidents[7]. To solve this problem, smart beam with an auto-controllable light field becomes an important component in revolutionary intelligent vehicles. They drastically enhance traffic safety and even enable human-vehicle communications. Traditional liquid crystal displays (LCDs)[8] and digital light processing (DLP)[9] are two typical techniques used to realize this concept, both of which can arbitrarily change the projected light patterns according to the road conditions. Until now, the former suffers from optical inefficiency due to the polarization-induced loss caused by the pair of polarizers, while the latter is cost inefficient and challenging in miniaturization. Therefore, it is of critical importance to develop new spatial light modulators with high optical efficiencies and large on-off ratios.

Liquid crystals (LCs) have received much attention thanks to their external field-controlled optical anisotropy and have been widely used in new optical technologies[10,11]. Large area and electrically controllable optical switches are adopted to provide comfortable and energy-saving working and living environments. LCs can efficiently modulate the transmittance and color of light, thus playing vital roles in the intelligent light regulation of buildings, vehicles, and airplanes[12–15]. Cholesteric liquid crystals (CLCs) are characterized by helical structures[16–20]. In vertically aligned or unaligned thick cells, the helical axes of CLCs are randomly oriented, leading to a strong scattering state. After a saturated electrical field is applied, the LC directors reorient normally to the substrates to form a transmissive homogeneous state. Light modulation can be carried out via switching between the two distinguished states[21]. An On-off ratio below 5 and a maximum transmittance up to 75% were presented[22]. Bistable smectic-A LC optical switches were reported based on the alternation between a transparent homeotropic state under a high-frequency electric field and a focal-conic scattering state induced by electrohydrodynamic instability under a low-frequency electric field. Operation voltages of 45–60 V are applied, the on-off ratio is 8.57, and the maximum transmittance reaches 86%[23]. A certain amount of monomer is mixed in LCs to form polymer dispersed liquid crystals (PDLCs)[24–27] or polymer stabilized liquid crystals (PSLCs)[28–34]. The main

difference between them is the concentration of the monomer. Typically, it is over 30% (mass fraction) for PDLCs. The plentiful monomers result in numerous spherical LC droplets dispersed in polymer holes. While it is usually below 10% (mass fraction) for PSLCs, the small amount of monomer turns to polymer networks that are surrounded by LCs after polymerization. Driven by an electric field, such devices can be switched between a high transmission state and a low transmission scattering state. The dye-doped LC strategy has attracted much attention because it can work without polarizers and thus significantly increases the optical efficiency. When black dye is introduced to LC, the orientations of dichroic dyes are guided by surrounding LCs due to the guest-host effect. It leads to a continuous change in transmittance and a high optical efficiency reaches 73%[35–38]. However, the on-off ratio of this strategy is limited to several tens, restricting the practical application in smart beams. Therefore, it is important to devise a new strategy for enhancing the on-off ratio while maintaining a high transmittance.

To overcome this limitation, we introduced UV polymerization to LC/dye/polymer composites and cured them at the electrically-driven homeotropic state. The combination of the scattering effect of CLC helixes and the absorption of black dye effectively suppressed the transmittance in the OFF state. When the CLC is electrically driven to a homogeneous state, the scattering disappears, and the absorption of black dye reduces significantly, leading to a high transmittance of nearly 80%. It improves the on-off ratio to over 280. Moreover, the spatial modulation of the incident white beam is demonstrated via electrically addressing a DDPSCLC cell. It provides a simple but efficient way to fabricate high-performance, all-visible light protection devices.

2. Principle and Fabrication

The absorption of a dichroic dye is strongly dependent on its long-axis orientation with respect to the incident linear polarization. It intensively absorbs light when the long axis is parallel to the linear polarization, while the absorption is effectively suppressed under perpendicular conditions. When a black dichroic dye is mixed with monomer-doped CLCs, it follows the random helixes of the CLC, forming a scattering state, as shown in Fig. 1(a–i). The dyes are randomly oriented by the host LCs and thus absorb light in a broadband omnidirectional manner. After a saturated voltage is applied, an electricity-induced homeotropic state is achieved [Fig. 1(a–ii)]. UV photopolymerization is carried out in this state, after which the DDPSCLC is formed [Fig. 1(a–iii)]. The polymer networks vertically align the surrounded LCs. Removing the applied voltage, the randomly oriented helixes recover [Fig. 1(a–iv)].

The precursor of the DDPSCLC consists of 96.3% (mass fraction) positive nematic LC (E7, $n_e = 1.646$, $n_o = 1.499$, $\Delta n = 0.147$, NCLCP, China), 0.7% (mass fraction) chiral dopant (R5011, NCLCP, China), 2% (mass fraction) polymer monomer (LC242, $n_e = 1.741$, $n_o = 1.571$, $\Delta n = 0.224$, NCLCP, China), and 1% (mass fraction) black dichroic dye (BD, HCCH, China). The surface-treatment-free cell is made of two indium tin oxide (ITO) glass substrates, and the cell gap is controlled by spacers. The LC mixture is capillary filled into the cell at 70°C, and the sample exhibits a haze state when cooled to room temperature. The incident light is strongly scattered due to the refractive index mismatch of the randomly oriented LC domains. The absorption and scattering together make the sample opaque. When observed under a polarized optical microscope (POM), focal-conic domains are revealed due to light scattering [upper micrograph in Fig. 1(b)]. When a saturated voltage is applied, all dyes reorient vertically, following the guidance of the LCs due to the guest-host effect. The high transmittance ON state appears as a dark state when observed under a POM with a pair of crossed polarizers [bottom micrograph in Fig. 1(b)]. The sample is immersed in acetone for 5 hours to wash out the LCs and then dried at room temperature for 4 hours. Then, we open the cell and characterize the sample by using a scanning electron microscope (SEM). Figure 1(c) confirms that the 2% monomer forms networks rather than polymer holes.

The transmittance spectra before and after UV photopolymerization are shown in Figs. 1(d) and 1(e), respectively. After UV photopolymerization, the average transmittance decreases from 12.8% to 0.25%. This is attributed to the polymer network increasing the randomness of the helix orientation and thus inducing much stronger scattering. When turned to the ON state, all molecules are vertically aligned and form a transparent state. The average transmittance in the ON state drops slightly. The on-off ratio (OR, $\mathrm{OR} = T_{\mathrm{on}}/T_{\mathrm{off}}$, where T_{on} stands for ON-state transmittance and T_{off} stands for OFF-state transmittance) increases drastically from 6.3 to 286.3 after UV polymerization. These differences can be vividly observed from the corresponding photographs, as shown in the insets of Figs. 1(d) and 1(e). The polymerization also increases the stability of the sample to external stress. In our experiments, samples become more transparent under a slight pressure before UV polymerization. However, they maintain strong scattering after UV polymerization, thanks to the LC reorientation that is inhibited by the polymer networks.

3. Experimental Results and Discussion

We systematically investigate the influences of dye concentration, chiral dopant concentration, and cell gap on the electro-optical properties of the DDPSCLC samples. First, four samples of different dye mass fractions (0%, 1%, 2%, and 3%) are fabricated with a fixed cell gap of 12 μm and a chiral dopant concentration of 0.7% ($p = 1.3\,\mu\mathrm{m}$). According to the voltage-dependent transmittance exhibited in Fig. 2(a), as expected, the transmittances in the OFF state decrease with the increasing of dye concentration due to the extra absorption introduced by the dye molecules. Dye absorption also induces a drop in transmittance in the ON state (from 83.1% to 70.7%). The dye concentration has little influence on the threshold and saturation voltages (20 V and 26 V, respectively) according to the curves. The inset in Fig. 2(a) indicates that OR increases to

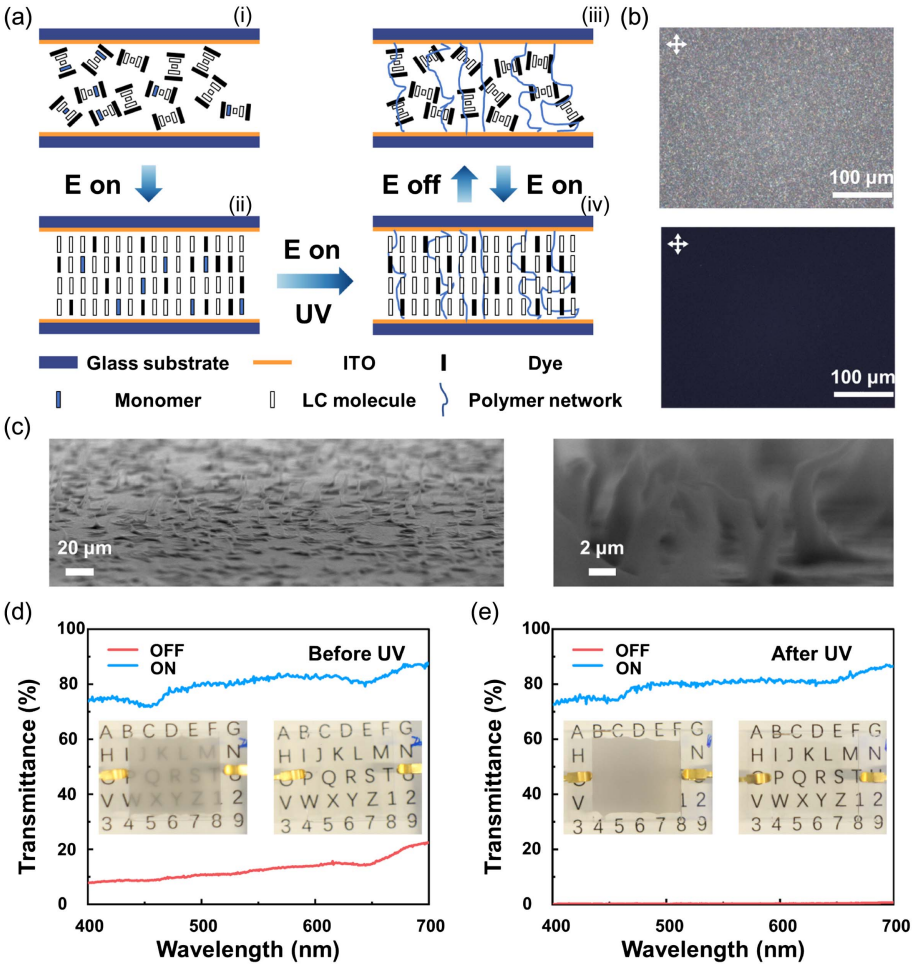

Fig. 1. (a) Fabrication of the DDPSCLC sample. (b) OFF-state and ON-state of the DDPSCLC sample observed under a POM with a pair of crossed polarizers. (c) 45° top view and side view SEM images of 2% monomer sample. Transmittance in wavelength range of 400–700 nm and corresponding images (inset) at OFF/ON states (d) before and (e) after the polymerization.

over 200 when dye is doped. For cost and energy efficient consideration, here we choose a dye concentration of 1%.

The chiral dopant concentration c and cell gap also affect the electro-optical property of the DDPSCLC sample. A series of DDPSCLCs with chiral dopant concentrations of 0.7%, 1.0%, 1.3%, and 1.6% was prepared. As shown in Fig. 2(b), along with the increasing of the chiral dopant concentration, the threshold and saturated voltages increase from 22 V to 56 V and 26 V to 58 V, respectively. Both of them increase significantly. According to the equation[39],

$$V_{\mathrm{th}} = \frac{d\pi^2}{p}\sqrt{\frac{K_{22}}{\varepsilon_0|\Delta\varepsilon|}}, \tag{1}$$

the threshold voltage is inversely proportional to the helical pitch p[39], $p = (1/\mathrm{HTP}) \cdot c$. The pitch of the CLC p means the distance that the LC director rotates is 2π along the helical axis. The saturated voltage increases accordingly. The ORs for the four samples are 286.3, 303.7, 284.7, and 216.0, respectively, which are all over 200. The scattering and absorption of these samples are comparable due to the similar morphology of the polymer network[40] generated under the same photopolymerization conditions. Here, 0.7% is selected due to the lower driving voltage and the long wavelength photonic bandgap that avoids unwanted visible color selectivity. Increasing the cell gap can also raise the OR. DDPSCLC cells with gaps of 5 μm, 12 μm, 15 μm, and 20 μm were fabricated. As revealed in Fig. 2(c), both threshold and saturated voltages rise with increasing cell gap (32 V and 36 V). In the OFF state, more scattering and absorption accumulate as the thickness increases. It induces a better dark state and thus facilitates the OR, which increases from 22.0 to 804.6 when the cell gap rises from 5 μm to 20 μm. Accordingly, the transmittance decreases slightly as well in the electrically driven homogeneous state (from 84.7% to 74.8%). A chiral dopant concentration of 0.7% and a cell gap of 12 μm are selected to reach an optimum tradeoff among the driving voltage, transmittance, and OR.

The ORs of the DDPSCLC samples with 1%, 1.5%, 2%, 2.5%, and 3% are shown in Fig. 2(d). As the monomer concentration

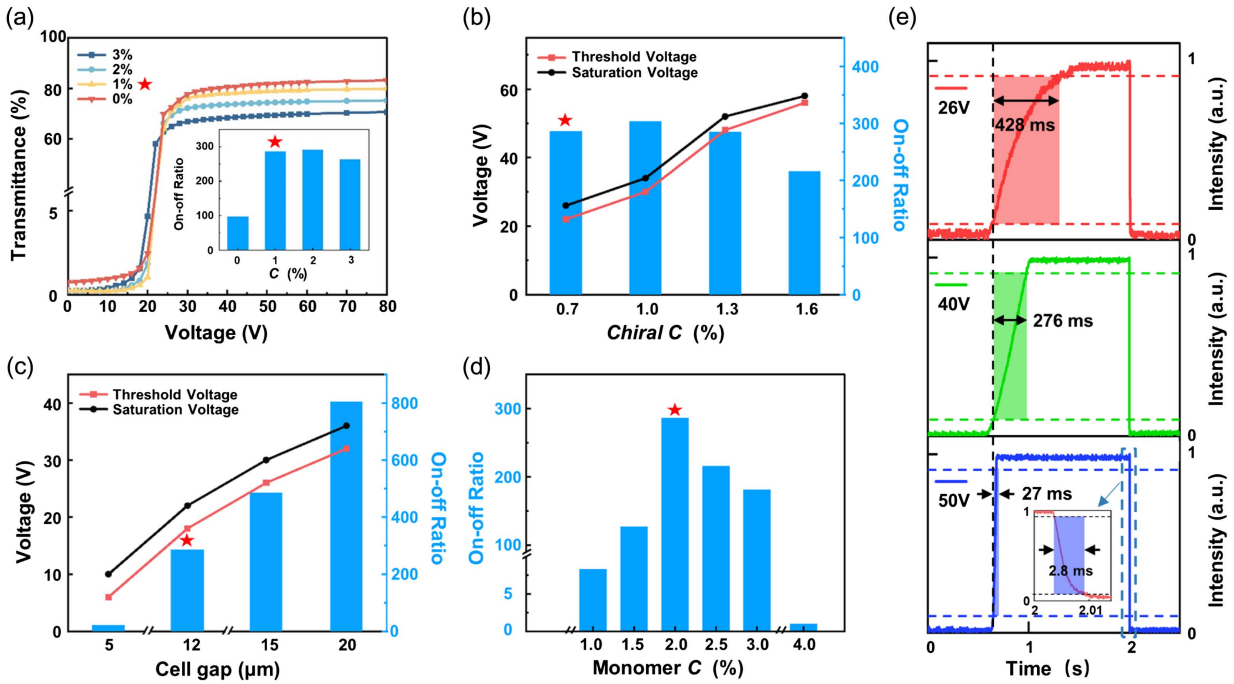

Fig. 2. Influences of different parameters on electro-optical properties of DDPSCLCs. (a) Voltage-dependent transmittance and on-off ratio (inset) of different dye concentrations (in mass fraction). Threshold voltage, saturation voltage, and on-off ratio of samples with different (b) chiral concentrations (in mass fraction) and (c) cell gaps. (d) On-off ratio of samples with different monomer concentrations (in mass fraction). The optimum condition is marked with a red star. (e) Voltage dependent response time of the sample with a chiral concentration of 0.7%, a dye concentration of 1%, and a cell gap of 12 μm.

increases from 0% to 2%, the OR rises from 8.3 to 286.3 due to the enhanced scattering from randomly oriented focal cone domains. Further increasing the concentration, more LCs are vertically aligned, and an opaque state is formed, leading to a decrease of the OR. When the concentration rises to 4%, all LCs are vertically aligned and a transparent state is presented. 2% is selected as the optimized value.

The response times τ_{on} and τ_{off} of the PSLC sample are expressed as follows[39]:

$$\tau_{on} = \frac{\gamma_1}{\varepsilon_0 |\Delta\varepsilon| E^2 - K_{22}\pi^2/P^2},$$
$$\tau_{off} = \frac{\gamma_1 P^2}{K_{22}\pi^2}. \quad (2)$$

γ_1 is the rotational viscosity of the LCs, and K_{22} is the twisted elastic constant. Figure 2(e) exhibits the voltage-dependent response of a DDPSCLC sample with 0.7% chiral dopant, 1% dye, and a cell gap of 12 μm. Here, the rise time is defined as the period in which the transmittance changes from 10% to 90%, while the reverse time is defined as the decay time. At a saturated voltage of 26 V, the rise time and decay time are 428 ms and 2.8 ms, respectively [Fig. 2(e)]. When the applied voltage increases to 50 V, the rise time decreases to 27 ms. According to Eq. (2) and Fig. 2(d), it is effective to improve the response by applying higher voltages. The decay time does not change along with the variation in voltage, as it is only determined by the elasticity and viscosity of the materials for a given cell gap.

Using a smart beam means that the intensity distribution of projected light can be freely programmed. For easy demonstration, a 5×7 pixelated electrode array with each electrode individually switched is fabricated. Figure 3(a) presents a photograph of the sample. Figure 3(b) schematically illustrates the detailed electrodes. The substrate is covered by patterned ITO electrodes, which are carefully designed to avoid interference among different units, while the superstrate is a common electrode. They are separated by 12-μm spacers and glued to form a

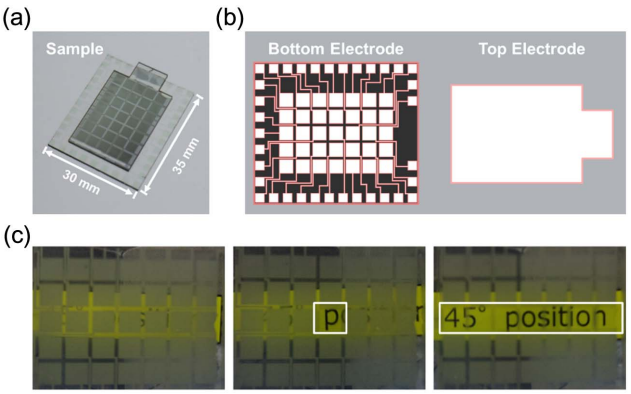

Fig. 3. (a) Electrically addressed DDPSCLC sample with 35 independent electrodes. (b) Designs for bottom and top electrodes. (c) Spatial switching of a selectively addressed DDPSCLC sample.

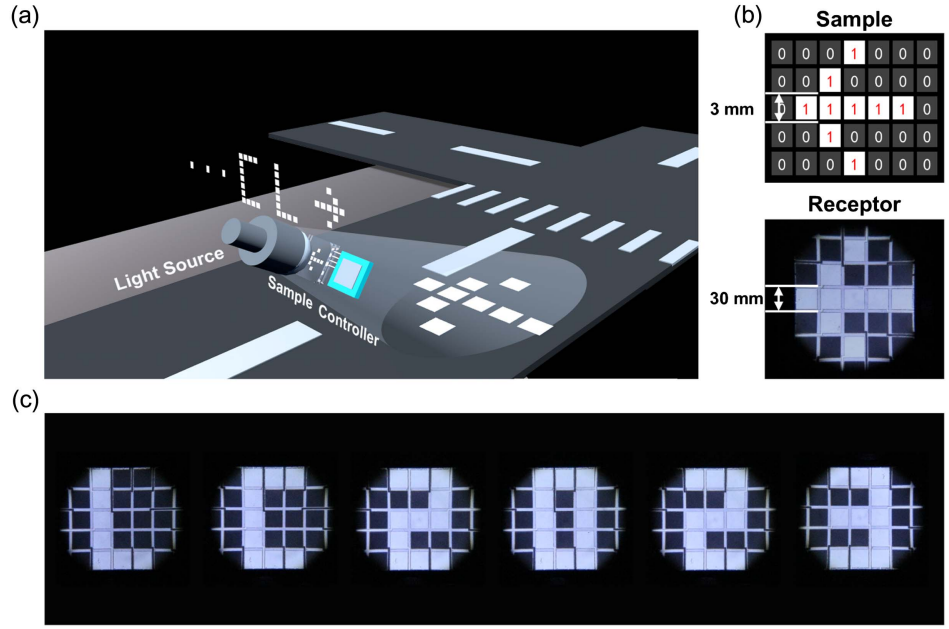

Fig. 4. (a) Schematic illustration showing the principle of the smart beam. (b) Voltages in the pixelated matrix and the pattern "arrow" on the receptor. (c) Switching effect of different voltage matrix patterns for the same sample.

cell. Figure 3(c) exhibits the spatial switching of the sample. The three images from left to right show the all opaque, single-pixel addressed, and row addressed states of the sample. All the background behind the OFF-state cannot be observed, while the information behind the ON-state pixels (26 V applied), such as the letters "p" and "45° position," can be clearly identified.

The smart vehicle lighting is schematically illustrated in Fig. 4(a). The white light emitted from an LED is reshaped by a free-form lens and then selectively shuttered by the DDPSCLC spatial light modulator. Finally, the beam carrying encoded information is projected onto the road. For example, a leftwards arrow is projected for demonstration in Fig. 4(b). In our experiment, the length of each pixel is expanded to 30 mm, which is ten times amplified. The carried information can be easily refreshed according to the driving conditions. Figure 4(c) presents six different letters and numbers to form "LC2023." The excellent tunability of the DDPSCLC sample enables a fast transformation of electric signals to optical patterns. Grayscale information displays are also reasonably anticipated, which will further promote the development of intelligent vehicles.

When 26 V is applied, which is below the general output voltage (28 V) of mainstream electric vehicles, transmittance over 70% with an OR $>$ 200 is achieved. The excellent performance makes DDPSCLC a practical candidate for smart beams. A prototype of a smart beam device is demonstrated by electrically addressing DDPSCLC with pixelated electrodes. Light patterns with arbitrary designs are projected dynamically. The performances satisfy the requirements of intelligent vehicles. Here, for easy demonstration, a 35-pixelated device is presented. Thanks to the mature manufacturing of LC devices, the dimension of a single pixel can be significantly reduced, while the total number of pixels can be drastically increased. The gaps between neighboring pixels can be reduced to further increase the optical efficiency. The design can be optimized to perfectly match the light source. In addition to the far beams of vehicles, the proposed design can also be adopted in vehicle tail lights, public information displays, advertising, and even AR/VR displays. The design suggests multiple effects can be simultaneously utilized to solve a problem when LCs featured by plentiful ordered structures and versatile functions are adopted.

4. Conclusion

A design for smart beams was proposed by electrically addressing a DDPSCLC spatial light modulator. It combines the scattering effect of randomly oriented CLC helixes and the absorbing effect of doped black dye and thus dramatically improves the OR while maintaining a high optical efficiency. A lighting device was demonstrated. Via pixelated addressing, different information is dynamically imprinted on the projected beams. This enhances driving safety and brings novel human-vehicle interactions, which may upgrade the performance of existing intelligent vehicles.

Acknowledgements

This work was supported by the National Key Research and Development Program of China (No. 2022YFA1203703), the National Natural Science Foundation of China (NSFC) (No. 62035008), and the Fundamental Research Funds for the Central Universities (No. 021314380233). The authors gratefully

thank Dr. Rui Yuan and Dr. Quanming Chen for their kind assistance in using their facilities.

References

1. F.-Y. Wang, "Metavehicles in the metaverse: moving to a new phase for intelligent vehicles and smart mobility," IEEE Trans. Intell. Veh. **7**, 1 (2022).
2. L. Chen, Y. Li, C. Huang, *et al.*, "Milestones in autonomous driving and intelligent vehicles: survey of surveys," IEEE Trans. Intell. Veh. **8**, 1046 (2023).
3. H. Wang, Y. Chen, Y. Cai, *et al.*, "SFNet-N: an improved SFNet algorithm for semantic segmentation of low-light autonomous driving road scenes," IEEE Trans. Intell. Transp. Syst. **23**, 21405 (2022).
4. S. E. Shladover, "Connected and automated vehicle systems: introduction and overview," J. Intell. Transp. Syst. **22**, 190 (2018).
5. V. Milanes, S. E. Shladover, J. Spring, *et al.*, "Cooperative adaptive cruise control in real traffic situations," IEEE Trans. Intell. Transp. Syst. **15**, 296 (2014).
6. X. Ouyang, J. Yang, Z. Hong, *et al.*, "Mechanisms of blue light-induced eye hazard and protective measures: a review," Biomed. Pharmacother. **130**, 110577 (2020).
7. R. Zhang, Z. Zhang, J. Han, *et al.*, "Advanced liquid crystal-based switchable optical devices for light protection applications: principles and strategies," Light Sci. Appl. **12**, 11 (2023).
8. H. W. Chen, J. H. Lee, B. Y. Lin, *et al.*, "Liquid crystal display and organic light-emitting diode display: present status and future perspectives," Light Sci. Appl. **7**, 17168 (2018).
9. H. Liu, H. Zhang, W. Han, *et al.*, "3D printed flexible strain sensors: from printing to devices and signals," Adv. Mater. **33**, 2004782 (2021).
10. Q. M. Chen, C. T. Xu, X. Liang, *et al.*, "Helical structure endows liquid crystal planar optics with a customizable working band," Adv. Quantum Technol. **6**, 2200153 (2023).
11. H. K. Bisoyi and Q. Li, "Liquid crystals: versatile self-organized smart soft materials," Chem. Rev. **122**, 4887 (2022).
12. V. K. Baliyan, K.-U. Jeong, and S.-W. Kang, "Dichroic-dye-doped short pitch cholesteric liquid crystals for the application of electrically switchable smart windows," Dyes Pigm. **166**, 403 (2019).
13. S.-H. Kim, S.-W. Oh, and T.-H. Yoon, "Enhancement of absorption and haze with hybrid anchoring of dye-doped cholesteric liquid crystals," Opt. Express **26**, 14259 (2018).
14. C.-C. Li, H.-Y. Tseng, C.-W. Chen, *et al.*, "Versatile energy-saving smart glass based on tristable cholesteric liquid crystals," ACS Appl. Energy Mater. **3**, 7601 (2020).
15. J. Yan, X. Fan, Y. Liu, *et al.*, "Passive patterned polymer dispersed liquid crystal transparent display," Chin. Opt. Lett. **20**, 013301 (2022).
16. Z. Zheng, H. Hu, Z. Zhang, *et al.*, "Digital photoprogramming of liquid-crystal superstructures featuring intrinsic chiral photoswitches," Nat. Photonics **16**, 226 (2022).
17. C. T. Xu, D. W. Zhang, R. Yuan, *et al.*, "Optical orbital angular momentum processors with electrically tailored working bands," Laser Photonics Rev. **17**, 2370031 (2023).
18. L. Wang, A. M. Urbas, and Q. Li, "Nature-inspired emerging chiral liquid crystal nanostructures: from molecular self-assembly to DNA mesophase and nanocolloids," Adv. Mater. **32**, 1801335 (2020).
19. C. T. Xu, B. H. Liu, C. Peng, *et al.*, "Heliconical cholesterics endows spatial phase modulator with an electrically customizable working band," Adv. Opt. Mater. **10**, 2201088 (2022).
20. C.-W. Chen, A. N. Brigeman, T.-J. Ho, *et al.*, "Normally transparent smart window based on electrically induced instability in dielectrically negative cholesteric liquid crystal," Opt. Mater. Express **8**, 691 (2018).
21. J.-H. Kim, J.-W. Huh, S.-W. Oh, *et al.*, "Bistable switching between homeotropic and focal-conic states in an ion-doped chiral nematic liquid crystal cell," Opt. Express **25**, 29180 (2017).
22. J.-M. Baek, S.-W. Oh, S.-H. Kim, *et al.*, "Fabrication of an initially-focal-conic cholesteric liquid crystal cell without polymer stabilization," Displays **52**, 55 (2018).
23. W. Ji, L.-Y. Shi, H. Tang, *et al.*, "Large birefringence smectic-A liquid crystals for high contrast bistable displays," Opt. Mater. Express **5**, 281 (2015).
24. H. Chen, H. Liang, W.-H. Lai, *et al.*, "A 2D/3D switchable directional-backlight autostereoscopic display using polymer dispersed liquid crystal films," J. Disp. Technol. **12**, 1738 (2016).
25. S. Guo, X. Liang, H. Zhang, *et al.*, "An electrically light-transmittance-controllable film with a low-driving voltage from a coexistent system of polymer-dispersed and polymer-stabilised cholesteric liquid crystals," Liq. Cryst. **45**, 1854 (2018).
26. Y. Xia, X. Liang, Y. Jiang, *et al.*, "High-efficiency and reliable smart photovoltaic windows enabled by multiresponsive liquid crystal composite films and semi-transparent perovskite solar cells," Adv. Energy Mater. **9**, 1900720 (2019).
27. X. Liang, M. Chen, S. Guo, *et al.*, "Dual-band modulation of visible and near-infrared light transmittance in an all-solution-processed hybrid micro–nano composite film," ACS Appl. Mater. Interfaces **9**, 40810 (2017).
28. W. Li, C. Yang, B. Luo, *et al.*, "Effect of preparation parameters on the performance of polymer-stabilized cholesteric liquid crystals for laser emission," Chin. Opt. Lett. **12**, 111602 (2014).
29. I. Dierking, "Polymer network-stabilized liquid crystals," Adv. Mater. **12**, 167 (2000).
30. Y. Zhang, Q. Zhan, C. Wang, *et al.*, "Unique polymer-stabilized liquid crystal structure prepared by addition of a reversible addition–fragmentation chain transfer agent," ACS Appl. Mater. Interfaces **15**, 51815 (2023).
31. Z. Li, R. Lan, J. Bao, *et al.*, "Tunable circularly polarized luminescence with a high dissymmetry factor emitted from luminogen-bonded and electrically controlled polymer-stabilized cholesteric liquid crystals," ACS Appl. Mater. Interfaces **14**, 8490 (2022).
32. J. Heo, J.-W. Huh, and T.-H. Yoon, "Fast-switching initially-transparent liquid crystal light shutter with crossed patterned electrodes," AIP Adv. **5**, 047118 (2015).
33. X. Hu, X. Zhang, W. Yang, *et al.*, "Stable and scalable smart window based on polymer stabilized liquid crystals," J. Appl. Polym. Sci. **137**, 48917 (2020).
34. B.-H. Yu, J.-W. Huh, J. Heo, *et al.*, "Simultaneous control of haze and transmittance using a dye-doped cholesteric liquid crystal cell," Liq. Cryst. **42**, 1460 (2015).
35. T. Zhan, J. Xiong, G. Tan, *et al.*, "Absorption-based polarization gratings," Opt. Express **28**, 13907 (2020).
36. X.-Y. Fan, W.-Y. Ma, Y.-M. Zhang, *et al.*, "Broadband spatial polarization processing of light via a photopatterned dichroic medium," Appl. Phys. Lett. **120**, 041103 (2022).
37. Y. Chen, Y. Zhang, H. Li, *et al.*, "Dynamic circularly polarized luminescence with tunable handedness and intensity enabled by achiral dichroic dyes in cholesteric liquid crystal medium," Adv. Mater. **34**, 2202309 (2022).
38. R. Gahrotra, V. Sharma, A. R. Dogra, *et al.*, "Performance augmentation of bistable cholesteric liquid crystal light shutter: effect of dichroic dye on morphological and electro-optical characteristics," Opt. Mater. **127**, 112243 (2022).
39. J. Ma, Z.-G. Zheng, Y.-G. Liu, *et al.*, "Electro-optical properties of polymer stabilized cholesteric liquid crystal film," Chin. Phys. B **20**, 024212 (2011).
40. Y. Deng, Y. Yang, Y. Xiao, *et al.*, "Ultrafast switchable passive radiative cooling smart windows with synergistic optical modulation," Adv. Funct. Mater. **33**, 2301319 (2023).